Rheological and Electrical Behaviour of [1]Nanocarbon/poly(lactic) Acid for 3D Printing Applications

Giovanni Spinelli[1*], Patrizia Lamberti[1], Vincenzo Tucci[1],
Radost Ivanova[2], Sonia Tabakova[2], Evgeni Ivanov[2,3], Rumiana Kotsilkova[2], Sossio Cimmino[4],
Rosa Di Maio[4], Clara Silvestre[4]

[1] *Department of Information and Electrical Engineering and Applied Mathematics*
University of Salerno, Via Giovanni Paolo II, Fisciano (SA) ITALY
[2] *Open Laboratory on Experimental Micro and Nano Mechanics, Institute of Mechanics,*
Bulgarian Academy of Sciences, Acad. G. Bonchev Str., Block 4, Sofia, Bulgaria
[3] *Research and Development of Nanomaterials and Nanotechnologies (NanoTech Lab Ltd.)*
Acad. G. Bonchev Str. Block 1, 1113 Sofia, Bulgaria
[4]*Istituto per i Polimeri, Compositi e Biomateriali, Consiglio Nazionale delle Ricerche*
Via Campi Flegrei 34 Olivetti, 80078 Pozzuoli (NA) Italy

* Corresponding authors. Fax:+39 089 964218 E-mail address: gspinelli@unisa.it;

Abstract. This paper aims to address current limitations of 3D printed conductive materials through the development of a novel formulation of a thermoplastic composite. In particular, a conductive filament suitable for three-dimensional printing is obtained on the basis of Polylactic acid (PLA) filled with two types of highly conductive nano-carbon materials, i.e. multi-walled carbon natotubes (MWCNTs), graphene nanoplates (GNPs) and a combination of both fillers (MWCNT/GNP). A systematic rheological and electrical characterization of the resulting nanocomposites is presented. Viscoelastic properties and rheological percolation threshold are determined for the binary and ternary composites and related to the size of nanoparticles. Comparable values for the percolation threshold are found by means of rheological and electrical studies. Low electrical percolation thresholds and high values of the electrical conductivity of the order of S/m are achieved for the investigated formulations. At the highest filler loading (i.e. 12 wt%) the electrical conductivity reaches the value of 4.54 S/m, 6.27 S/m and 0.95 S/m for the composites based on MWCNTs, GNPs and multiphase system, respectively. These results, together with the good stability shown

by the nano-reinforced PLA in the frequency range [100Hz-1MHz] make these composites as promising candidates for 3D printed conductive devices for electromagnetic (EM) applications.

Keywords: Additive manufacturing; nanocomposites; 3D printing; carbon-based materials.

1. Introduction

Carbon-based fillers such as carbon nanotubes (CNTs), nanofibers (CNFs) and graphene possess excellent electrical conductivity together notable mechanical and thermal properties [1, 2]. When such nanoparticles are introduced in host polymeric matrices, the interesting properties of these latter (like easy processability and shaping possibilities, resistance to corrosion, flame, moisture, etc.), are enhanced giving rise to nanocomposites that recently have gained great attention from both academicians and industries. In fact, these innovative composites can leverage many of these combined properties leading to develop new materials for several applications ranging from aeronautic, automotive, plastics, semiconductor and electronic industrial sectors [3, 4]. Experimental investigations and theoretical studies with an eye toward the development of new fabrication processes and suitable functionalization may provide suitable indications in order to extend the applications range of nanocomposites. A recent research field paralleling the development of nanocomposites concerns the three-dimensional printing (3DP) also known as additive manufacturing (AM). With this approach computer-aided design (CAD) specifications allow the creation of 3D objects whose shape can be more complex than conventionally machined parts [5]. In fact, 3DP allows fast and accurate fabrication of structures having complex 3D features and sizes ranging from sub-micrometer to several meters, thus favoring low cost rapid prototyping [6]. Otherwise, the accuracy of geometries and the functionality of final products are limited by the capabilities of the tools used in manufacturing processes. The introduction of nanotechnology into this innovative field offers huge potential and opportunities for the manufacturing of 3D designed materials with customizable properties and specific multifunctionality [7, 8]. In particular, the interest in adding nanomaterials into the host matrix aims to improve the sintering characteristics and the mechanical, thermal and electrical properties of the resulting structures [9, 10]. In pioneering experiments, different metal nanoparticles of iron, gold or silver have been utilized because the melting temperature, due to the thermodynamic size effect, can be significantly reduced. Consequently, lower temperatures are required to sinter and extrude the printed parts, thus improving the quality of the final product [11, 12]. Among the different types of 3D printing techniques, such as selective laser sintering (SLS) [13], solvent-cast 3DP (SC3DP) [14], UV-assisted 3DP (UV3DP) [15], stereo-lithography [16], the fused deposition modeling (FDM) seems to be one of the most

promising fabrication methods developed so far [17,18]. Thanks to the carbon nanocomposites, this approach allows to overcome the challenge of 3D printing of electrically conductive materials. In fact, the previously used conductive materials, like metals, were not suitable as a feeding material for such 3DP method where melting and extrusion from a nozzle has to be ensured. Nowadays, in the midst of a growing demand for multifunctional devices, 3D printing conductive materials have shown their potential for various applications, such as electrical interconnections [19], electrochemical systems [20, 21], antennas [22], sensors [23] and so on up to a recent micro Li-Ion battery using an optimized ink with suitable composition and rheology [24]. In fused deposition modeling (FDM), for 3D printing of conductive polymer nanocomposites the feedstock is generally a thermoplastic polymer filament reinforced with different carbon-based particles, which is heated above its glass transition temperature (Tg), then extruded and deposited to form the desired 3D structure. However, despite significant successes, various challenges in the application of nanotechnologies to AM techniques remain to be faced.

Adhesion of polymer and nanocomposite layers, which were 3D printed with FDM technique directly onto the textile fabrics, was investigated. In particular, different variables which may affect the adhesion properties including 3D printing process parameters, fabric type and filler type incorporated in polymer were considered [25]. Polylactic acid (PLA) and graphene reinforced polylactic acid (PLA-graphene) composites have been fabricated by fused deposition modeling (FDM) printing and indentation creep resistance was analyzed in terms of the strain-rate sensitivity index [26]. Experimental characterization and micrography of 3D printed PLA and PLA reinforced with short carbon fibers are reported in [27]. The preparation and characterization of conductive PP-based thermoplastic composites suitable for electrical circuit printing using FDM-based 3D printing is described in [28] with particular interest to assess the reliability of 3D-printed prototypes generated from these conductive filaments, after different stress-tests (UV irradiation, thermal, and electrical).

Therefore, several critical factors, among which the proper choice of the materials and their suitable formulation and functionalization, must be take into account to achieve control of properties of the final product in terms of electrical and thermal conductivity, mechanical strength, and stiffness [29, 30]. Moreover, it is important to overcome some well-known limitations, such as nozzle clogging, aggregation within printing media, potential warping or curling as well as poor esthetics due to high surface roughness of printed parts. Therefore, more research efforts need to be produced to achieve totally the mutual benefits of nanotechnology and AM. An analytical optimization of a

nanoparticle of microstructural fused deposition of resins has been proposed in an attempt to enhance productivity of such 3D printing technology [31].

The work presented here aims to address current 3D printing limitations through the development of a novel formulation of nanocarbon/poly(lactic) acid with improved electromagnetic properties with respect to commercial filaments adopted for three-dimensional printing. The choice of PLA as base thermoplastic polymer arises from the need to promote, at the same time, sustainable composite materials combining good stiffness, strength and ductility in the perspective of a positive environmental footprint [32]. In particular, binary and ternary thermoplastic composites of Polylactic acid (PLA) filled with two types of highly conductive nano-carbon materials, i.e. multi-walled carbon nanotubes (MWCNTs) and graphene nanoplates (GNPs) and a combination of both fillers are considered. The filler contents and aspect ratio may have a relevant impact on the complex viscosity. This interesting aspect has been discussed in a previous paper [33]. In particular, by adopting three different techniques for estimation of the rheological percolation threshold, it is found that the larger the aspect ratio of filler, the lower is the rheological percolation threshold. In the present work, a systematic rheological and electrical characterization of the resulting nanocomposites is presented. Evaluation of the viscoelastic features and electrical properties in terms of percolation threshold, DC and AC electrical conductivity, impedance analysis are carried out in order to exploit their plausible use as basic materials for 3D printing object for electromagnetic applications. High electrical conductivity achieved with low amounts of filler and a good stability of the electrical properties in the frequency domain are favorable elements for the creation of 3D physical objects whose potential complex shape allowed by computer-aided design can strongly improve their electromagnetic (EM) interference shielding efficiency (EMI SE) thus making them particularly attractive for solving electromagnetic compatibility (EC) problems [34].

2. Materials and methods

2.1 Materials

The poly(lactic) acid (PLA) polymer used in this study was Ingeo™ Biopolymer PLA-3D850 (Nature Works) with MFR 7-9 g/10 min (210°C, 2.16kg, according to D1238 ASTM Method). Graphene Nanoplates (GNP) with purity 90 wt.%; diameter < 5 μm; aspect ratio ~240 and multiwall carbon nanotubes (MWCNTs) having purity 95 wt.%, outer diameter 30 nm, inner diameter 5-10 nm, length >10μm, aspect ratio ~1000, were supplied from Times Nano, China (commercial code: TNIGNP and TNIMH4 for GNP and MWCNT, respectively). Three types of nanocomposite materials, binary nanocomposites of GNP/PLA and MWCNT/PLA, as well as ternary systems

GNP/MWCNT/PLA with ratio 50:50 of GNP to MWCNT and variable filler contents from 0 to 12 wt.% were prepared by melt extrusion at temperatures 170-180ºC and screw speed 40 rpm. Twin screw extruder (COLLIN Teach-Line ZK25T) was used to produce pellets of nanocomposites. The filament extrusion from nanocomposite pellets was performed by single screw extruder (Friend Machinery Co.) at 10 rpm within temperatures 170-180ºC. The extrusion conditions were prior optimized in order to avoid both considerable break of nanofillers and thermo-mechanical degradation of PLA polymer; the latest was controlled by the PLA viscosity before and after extrusion. Based on the results showing the negligible variation of the viscosity, it can be concluded that the aspect ratio of the MWCNTs does not change significantly.

Fig. 1 shows the adopted extruder (Fig. 1a), the obtained filaments (Fig. 1b) and the 3D printer (Fig. 1c) used to manufacture the samples characterized in this study in order to explore the benefits of nanotechnology and AM for 3D printing of conductive materials.

2.2 Experimental methods

The rheological measurements were performed using AR-G2 Magnetic Bearing Rheometer (TA Instruments) with parallel-plate geometry (steel plates diameter 25 mm) using low amplitude oscillatory shear mode. Dynamic viscosity η', storage modulus G' and loss modulus G'' were measured versus the angular frequency, ω in the range 0.01 – 100 rad/s at strain amplitude of 0.1% (for 6-12wt% filler contents) and 0.5% (for 0-3wt%) and gap size of 500 μm between the plates. The G'-value is a measure of the energy stored by the material during the deformation cycle and represents the elastic behavior of the material, while G'' concerns the energy dissipated or lost as heat during the shear process and represents the viscous behavior of the tested material. The linear viscoelastic range of the strain amplitude was initially determined by strain sweep test at the angular frequency of 1 Hz. Example results for the storage modulus versus applied strain are shown in Figure 2. All rheological measurements were performed at a temperature of 200° C. The TA Advantage Software was used for data analysis.

For the analysis of the structure and morphology, bright field transmission electron microscopy (TEM) analysis was performed by using FEI TECNAI G12 Spirit-Twin (LaB6 source) instrument equipped with a FEI Eagle-4k CCD camera and operating with an acceleration voltage of 120 kV. The analysis was performed on sections obtained at room temperature by using a Leica EM UC6/FC6 ultramicrotome. The sections were placed on 400 mesh copper grids. The measurements of the DC volume conductivity of the composites were performed by using

disk-shaped specimens of about 1 mm thickness and 50 mm diameter. Before performing the electrical measurements, the samples are thermally pre-treated at 40 °C for 24 h. Then, both the sides of the samples have been metallized (circular form of about 22 mm of diameter) with silver paint (Alpha Silver Coated Copper Compound Screening, with a thickness of about 50 mm and a resistivity of 0.7 Ω-square) in order to reduce the effects of eventual surface roughness and to ensure ohmic contacts. The measurement system is composed by a multimeter Keithley 6517A with function of voltage generator (max ± 1000 V) and voltmeter (max ± 200 V) and an ammeter HP34401A (min current 0.1 fA). The AC properties were determined in the frequency range 100 Hz–1MHz by using a Quadtec7600 dielectric analyzer. Five samples were prepared and then tested for each composition. For the sake of graphic clarity, the electrical data reported as results are the average values. All electrical measurements were carried out at room temperature.

3. Results and discussion

3.1 Rheological behavior

The rheological behavior in dynamic test mode of the three nanocomposite types has been studied and compared with the neat PLA. Figure 3(a,b) presents experimental data for the storage modulus, G', versus angular frequency, ω for: (a) binary GNP/PLA and (b) binary MWCNT/PLA and ternary GNP/MWCNT/PLA composites, as varying the filler contents from 0 to 12 wt%. As seen, the viscoelastic behavior on the neat PLA polymer in the terminal region, ω→0 may be described by scaling of the storage modulus $G' \sim \omega^2$ with the power law slope n = 2. When nanoparticles of GNP and MWCNT are added to the PLA, a non-terminal behavior was observed. In fact, the power law slope *n* gradually decreases by increasing the nanoparticle content, as shown in Table 1.

Theoretically, the slope value of the power law of gel-like structures is around n ~ 0.5, that is usually associated with percolation [35]. The slope values related to percolation, according to the gel-like model is achieved in our study between 6 - 9 wt% for GNP/PLA (n = 0.924 - 0.437); around 1.5 wt.% for MWCNT/PLA (n = 0.527); and below 3 wt% for the ternary composites (1.5%GNP/1.5%MWCNT/PLA, with n = 0.327), respectively. As seen, the nanocomposite MWCNT/PLA demonstrates the lowest percolation, which may be associated with the high initial aspect ratio of carbon nanotubes and their better dispersion in the PLA matrix, compared to the GNP. The ternary GNP/MWCNT/PLA nanocomposite (in ratio 50:50 of MWCNT and GNP) show percolation between those of the two binary nanocomposites. The changes of the low frequency terminal storage modulus, G_o' with increasing the

nanoparticle concentration, ϕ, was considered in order to study the efficiency of the carbon nanofillers GNP, MWCNT and their mixture GNP/MWCNT to transform the viscoelastic behavior of PLA polymer. In Figure 4, data obtained for G_o' = f(ϕ), were plotted for the three nanocomposite types: binary systems (GNP/PLA and MWCNT/PLA), and the ternary system GNP/MWCNT/PLA.

The experimental points for the three nanocomposite types in Fig. 4 were fitted to the fractal model (Eq.1), above the starting point (ϕ_p) for the appearance of the scaling law [36]:

$$G_o' \sim \phi^{m} \quad (1)$$

where, G_o' is the terminal storage modulus at ω = 0.2 rad/s which values are summarized in Table II; ϕ is the weight fraction of the filler and m is the scaling exponent. The following main differences are observed in Fig. 4 for the three nanocomposite types:

- First, the critical filler concentration (ϕ_p) that is the starting point for the appearance of the scaling law is different for the three types of nanocomposites, due to different size, shape and the state of dispersion of nanoparticles. The starting point ϕ_p is usually related to the rheological percolation threshold, where a continuous network is formed by interconnected nanoparticle aggregates, immobilized with matrix polymer (called fractals) [37,38]. As seen from Fig. 4, the rheological percolation, determined by this criteria (starting point for the appearance of the scaling law) is of ϕ_p = 5.02 wt.% for the GNP/PLA nanocomposite. However, for other two composite types the percolation threshold obviously appear below the lower concentration limit studied, thus $\phi_p \leq$ 1.5 wt.% for MWCNT/PLA and $\phi_p \leq$ 3 wt.% for the GNP/MWCNT/PLA nanocomposites could be proposed.

- Second, the plots in Fig. 4 demonstrate that the scaling law exponent (m) of $G_o' \sim \phi^m$ differs for the three nanocomposite types, which may be associated with different size of fractals formed above the percolation threshold [35,37]. Fractals are accepted herewith as agglomerates of similar size and structure that are formed by carbon nanoparticles and immobilized polymer layer in between. Thus, the scaling law slope (m = 8.144) was calculated for the GNP/PLA, that is much higher than that for the MWCNT/PLA (m = 3.077). The ternary GNP/MWCNT/PLA composite show slope m = 3.429, which is similar to that of the MWCNT/PLA. With reference to the fractal theory [39] the fractal dimension (D) was related to the scaling law exponent by the following Eq. (2),

$$G_o' \sim \varphi^{5/(3-D)} \quad (2)$$

where, the scaling law exponent is presented by m = 5/(3 - D), with D representing the fractal dimension.

Based on this concept, and using the values of the scaling exponent pointed out in Fig. 4, the fractal dimensions were calculated of D = 2.386 (for GNP/PLA), D = 1.375 (for MWCNT/PLA) and D = 1.542 (for GNP/MWCNT/PLA). Obviously, the fractals formed in the three nanocomposite types have different dimensions due to the different size, shape and degree of dispersion of the dispersed nanoparticles. Thus, the GNP nanoplatelets (with lower initial aspect ratio ~240) seem to form twice larger fractals compared to those formed by MWCNT nanotubes (with higher initial aspect ratio ~ 1000), which can be associated with a better dispersion of MWCNTs compared to GNP in the PLA matrix. While the fractal dimensions in the ternary nanocomposites at ratio 50:50 of GNP/MWCNT coincide with that of binary nanocomposites with MWCNTs, confirming the similar degree of dispersion of the mixed GNP/MWCNT fillers (at 50:50 ratio) in PLA polymer above the percolation threshold.

3.2 Structure and morphology

The images in Fig. 5a, Fig. 5b show the TEM micrographs of an example ternary 6wt% nanocomposite GNP/MWCNT/PLA, containing 3 wt.% GNPs and 3 wt.% MWCNTs at different magnifications: (a) low magnification scale of 500 nm and (b) high magnification scale of 200 nm. In Fig. 5a, homogeneous dispersion of MWCNTs in the PLA polymer is visualized where nanotubes are dispersed to single particles or small aggregates. While, at high magnification in Fig 5b, it is seen that the microstructure of nanocomposite consists of lots of small fractals of size < 200 nm (marked with the smaller circle), that are formed by the dispersed MWCNT in the PLA polymer. A few larger fractals (300-400 nm, marked with the larger circle) are visible, containing both nanofillers, GNP and MWCNT. In contrast, the GNP nanoplates form large asymmetric fractals of length >1000 nm and width >300 nm (marked with the ellipse) in the PLA matrix.

It is very likely that the nature of the attractive interactions between the carbon-based nanofillers and the polymeric matrix is due to the interaction between the oxygen atoms of PLA and polar groups (-OH, -COOH, etc..), which are always present as defects on the edges of GNP nanoparticles and the terminal parts of MWCNTs (as also reported in the Data Sheet provided by the manufacturing Company). These interactions could be responsible of the good level of dispersion observed in TEM micrographs for both fillers in Fig. 5.

It may be concluded that the rheological calculations for the fractals dimension above the percolation threshold, combined with the TEM images structure and morphology may be applied for evaluation of the printability of the three nanocomposite types by 3D printing (fused deposition modeling). Thus, the binary GNP/PLA nanocomposite

filament at filler contents above percolation, ϕ_p = 5.02 wt.% may produce clogging in the nozzle during extrusion, due to the large size of fractals formed by the graphene nanoplatelets in the matrix PLA. While such problem could not appear in the 3D printing (FDM) of binary MWCNT/PLA and ternary GNP/MWCNT/PLA nanocomposite filaments, due to the twice smaller fractal size of their aggregates.

3.3 DC Electrical properties

The DC electrical conductivity and percolation threshold of the composites have been investigated. In particular, in Fig. 6 the variation of the bulk conductivity of the composites is reported as a function of increasing filler content (wt. %) for the two types of nanoparticles (i.e. MWCNTs & GNPs) considered in the present study.

It can be observed that there are some remarkable differences between the two resulting nanocomposites. First of all, the percolation threshold (*EPT*), i.e. the minimum amount of conducting filler allowing to form a continuous path within the insulating polymer matrix and a consequent steep increase in conductivity values falls, at least for the investigated concentrations, in the range [1.5÷3] wt.% and in the range [3÷6] wt% for nanocomposites filled with MWCNTs and GNPs, respectively. The difference could be related to the dissimilar physical features of the two fillers. Several experimental and theoretical studies have been focused on identification of the critical factors that affect the percolation threshold of conducting polymer composites. Based on excluded volume theory [40] and numerical simulations [41], strong correlations were identified between the percolation threshold (*EPT*) and aspect ratio (*AR*) of fillers. In particular, it is observed that the electrical percolation threshold decreases with increasing the aspect ratio in agreement with the following expression: $EPT \propto 1/AR$. This difference in *EPT* may be justified in the light of this predicted trend and the information reported in the previous section "2.1 Materials" concerning the aspect ratio of the adopted fillers (i.e. 230 and 1000 for GNPs and MWCNTs, respectively) since the lower is the aspect ratio, the higher is the percolation threshold. Instead, for multiphase composites loaded with both fillers (i.e. PLA/MWCNTs&GNPs) the percolation threshold falls in the interim range of [3÷6] wt%. It is worth to note as the values of the percolation thresholds found by exploring electrical properties agree very well with those determined by rheological studies. Therefore, a close relationship between the two properties of the nanocomposites [42-44] exists, although the rheological properties were measured in the molten state of the resin while the electrical conductivity was measured on "solid" samples at room temperature. As the concentration of the conductive fillers

(i.e.ϕ) approaches the EPT, the electrical conductivity of the composites increases significantly with respect to that of the pure resin following a scaling power-law of the form:

$$\sigma=\sigma_0(\phi-\phi_n)^t \quad (3)$$

where σ_0 is the intrinsic conductivity of the filler, ϕ_n is the electrical percolation threshold (i.e *EPT*) and t is a critical exponent depending on the dimensionality of the percolating structure. It is ascribed to formation of an interconnected electrical network among the neighboring nanoparticles providing a continuous pathway for the electrons within the polymer thus causing a transition from insulator to conductive behavior [45]. In particular, the DC conductivity at a loading of 3 wt% for MWCNTs reinforced composite reaches the value of about 1.31×10^{-2} S/m, whereas samples of epoxy resin filled with GNPs are still below the percolation threshold since they present an electrical conductivity of pS/m that is close to the value of the neat polymer. The multiphase composite based on both fillers (i.e PLA/1.5wt% GNPs/ 1.5wt% MWCNTs) shows an electrical conductivity of 5.03×10^{-7} S/m that is above the EPT, being this value almost five order of magnitude higher than that of pure PLA. Finally, at the highest filler loading (i.e. 12 wt%) the electrical conductivity reaches the value of 4.54 S/m, 6.27 S/m and 0.95 S/m for the composites based on MWCNTs, GNPs and MWCNTs/GNPs respectively. All data regarding the electrical conductivity values are summarized in Table 3.

The plot of conductivity versus the fillers content in Fig.6 shows comparable values also in terms of electrical percolation thresholds with the electrical results reported in [46] carried out on non-conventional polymer nanocomposites (CNT- and graphene-based polybutylene terephthalate (PBT)) proposed for printing of electrically conductive structures by means of FDM technology. Instead, an evident improvement of the electrical properties is observed if our results are compared with those reported in [47] carried out on nanocomposites based on the same type of thermoplastic polymer (PLA) and reinforcement (CNTs). Such differences could be justified considering that many parameters such as the aspect ratio, the dispersion level and presence of agglomerates, the fabrication process, the nature of the matrix and its interaction with the fillers, have been proposed to affect the overall performances of the resulting materials. For example the CNTs adopted in [47] being produced by an other manufacturer, differ in shape respect to those adopted in the present study as well as, for the same reason, the matrix could have different crystallinity and so on.

Moreover, as shown in Fig. 7a, 7c, 7e, the characteristic parameters of the percolation law can be estimated for each percolation curve, by reporting the log–log plots of the experimental conductivity versus filler concentration. In

particular, the value for the critical exponent *t* can be obtained as the slope of the linear fit. Instead, the value of the estimated electrical percolation threshold (i.e. $\phi_{n\ estimated}$) is used as a variable parameter to maximize the regression coefficient (i.e. $R^2 \rightarrow 1$) of each interpolating curve. As it concerns the exponent *t*, the estimated values, i.e. 2.1, 1.3 and 1.5 for composites reinforced with carbon nanotubes (MWCNT/PLA), graphene nanoplates (GNP/PLA) and both fillers (GNP/MWCNT/PLA) respectively, are found to agree with the universal values observed for composites in which the conductive fillers form a continuous bi-dimensional or three-dimensional percolating path throughout the matrix, depending on the type, size, and geometry of the nanoparticle [48]. In particular, the higher value of *t* for MWCNTs reflects an effective 3D organization of the percolating structure consistent with 1D type of such filler, whereas for composites filled with GNPs, due the two-dimensional shape exhibited by these nanoparticles, the scaling exponent decreases significantly. Such a result has been already observed by *Guadagno et al.* in a study focused on new modified epoxy formulations based on different carbon nanofillers [49]. The estimated electrical percolation thresholds (i.e. 2.3 wt%, 5.5wt% and 3 wt%, for MWCNT/PLA, GNP/PLAand GNP/MWCNT/PLA, respectively) fall perfectly in the ranges identified by the experimental characterization. The change in the electrical conductivity of the composite materials, when the electrical percolation threshold is reached in coincidence with the formation of a conductive path inside the material, can be interpreted in terms of electron tunneling. According to this model the electrons ‘‘jump’’ from a conductive particle to the closest one over a small distance of the order of a few nanometers [45]. Such conduction mechanism can be modeled with a resistance R_{tunnel} given by the following expression:

$$R_{tunnel} = \frac{h^2 d}{Ae^2\sqrt{2m\lambda}} exp^{\left(\frac{4\pi d}{h}\sqrt{2m\lambda}\right)} \quad (4)$$

where *h* is the Plank’s constant, *A* and *d* are the cross-sectional area and the distance between the filler (coincident with the thickness of the insulating resin wrapped around the particles) respectively, *e* is the electron charge, *m* is the mass of electron and λ is the height of barrier, typically of few eV. A method reported in literature [50-52] to verify that the electron tunneling is the main electrical transport mechanism in such nanofilled resins is based on the occurrence of a linear relation (see Fig. 7b, 7d, 7f) between the electrical conductivity (in natural logarithmic scale) and $\phi^{-1/3}$, valid for concentrations (ϕ) above the EPT, i.e.:

$$ln(\sigma) \propto \phi^{-1/3} \quad (5)$$

The straight lines are fit curves of the experimental data (markers): the value of R^2 very close to 1 confirms that the electrical conduction network in nanocomposites materials is mainly achieved through the quantum tunneling effect.

As a consequence and in agreement with the parameters of the tunneling equation (eq. 4), the current and therefore the electrical conductivity of the resulting nanocomposites is related not only to the intrinsic features of the adopted filler but, depending on the dispersion technique and manufacturing process, also to its interaction within the host matrix and interfacial effects. These in turn affect the final interparticle distances and height of barrier. For this reason, many research efforts are devoted to the development of a controllable production process in order to achieve specimens with customized and comparable overall performances.

Some of these electrical aspects have been also numerically investigated by using a 3D simulation model developed by the authors in order to predict the electrical properties of carbon-based filled composites [41, 46, 53]. In Fig. 8a, it can be observed that also numerical analysis reveals that the EPT decreases with increasing of the aspect ratio of the filler in accordance with theoretical prediction (the so called Excluded Volume Theory) providing also upper and lower bounds for the expected formation of electrical paths (in the graphic, dashed and continuous line, respectively) [40, 41]. As evident from Fig. 8b the AR plays a key role even in determining the overall electrical conductivity of the resulting nanocomposites, In fact, for the same amount of fillers, an appreciable improvement of the conductivity appear with the increasing of the aspect ratio. Most likely, it is due to the enlargement of the interface area, which in turn affects the interaction with the host resin and consequently improve the dispersion state of the filler thus favoring the electrical percolation network [53].

3.4 AC Electrical properties

New advanced materials such as nanocomposites whose properties may be tailored by acting on the shape and content of the adopted fillers are promising candidates for electromagnetic (EM) applications such as shields, filters and radar absorber materials (RAMs). Therefore, the experimental investigation on the AC electrical properties of carbon-based nanocomposites is required in order to evaluate their effectiveness for such purposes. A technique classically adopted to this aim is the impedance spectroscopy (IS) based on measurement and evaluation of the electrical impedance or permittivity and electrical conductivity, as a function of the frequency (i.e. f) of the applied voltage.

In a simplified analysis at macro-scale, the AC properties of the polymer/carbon based composites can be described by using an equivalent model (Fig. 9) with single time-constant (TC) whose overall impedance is given by the

parallel combination of a resistor (*Rp*) and capacitor (*Cp*). Its analytic expression as function of the angular frequency, i.e. ω=2πf, is reported as Eq. 6.

Briefly, *Rp* and *Cp* take into account the electrical resistance of the material mainly due to the conductive percolating network and the capacitive effects related to the dielectric behavior of the resin, respectively [46].

$$|Z| = \frac{R_p}{\sqrt{1+\omega^2 R_p^2 C_p^2}}, \quad \varphi = arctg(\omega R_p C_p) \tag{6}$$

Fig. 10 shows the normalized impedance with respect to the thickness (Ω/m) of the sample (Fig. 10a), of the relative phase (in degree, Fig. 10b), the AC electrical conductivity (Fig. 10c) and real part of dielectric permittivity (Fig.10d) of the nanocomposites evaluated in the frequency range from 100Hz up to 1MHz. Although the frequency analysis is carried out for all specimens, for the sake of clarity of the graphs, the reported results concern only two specific concentrations for each type of investigated system, i.e. GNP/PLA, MWCNT/PLA, GNP/MWCNT/PLA. These concentrations have been chosen since one of them is below and the other is above the electrical percolation threshold for the specific system. In addition, as a reference, the behavior of pure PLA is presented.

As it concerns the electrical impedance (Fig. 10a and Fig. 10b), it is worth noting that for composites below the percolation threshold the $|Z_{norm}| \propto 1/f$ (i.e. a straight line in log-log scale), whereas the phase $\varphi \cong -90°$, as expected for insulating materials where charge transport cannot take place due to the lack of a conductive network. Vice versa, for nanocomposites with filler concentrations above the EPT, in the investigated frequency range, both the modulus and phase exhibit a value almost constant (zero for the phase), typical of a resistive material due to the setting of conducting paths.

Moreover, with regard to the AC conductance (Fig. 10c), first of all it can be seen as at low frequency (i.e. 100Hz), the value of AC conductivity of composites above EPT is close to that measured in DC. For composites below the percolation threshold, the electrical conductivity shows an evident frequency dependent behaviour similar to that observed for the pure PLA. In particular, a progressive growth of the conductivity with increasing frequency is observed due to the increasing contribution due to the frequency dependent displacement current associated to the capacitance in Fig. 9.

For composites above the EPT there is a frequency independent conductivity almost in the investigated frequency range [100Hz-1MHz]. For such materials, starting from a certain critical frequency f_c, the AC conductivity increases with a behaviour that can be described by an Almond-West-type power law [54, 55]:

$$\sigma(\omega) = \sigma_{DC} + A \cdot \omega^{s} \quad (7)$$

where σ_{DC} is the DC conductivity, $A \cdot \omega^{s}$ is the AC conductivity. In particular, A denotes a constant dependent on temperature, and s is a characteristic exponent whose value is strictly close to 1.

Another important properties that plays a key role especially as concern the design for electromagnetic purposes is the dielectric permittivity usually represented as the complex value of:

$$\varepsilon = \varepsilon' + i\varepsilon'' \quad (8)$$

where ε' and ε″ are the real and imaginary parts, respectively. More in details, the real part of the dielectric permittivity is related to the displacement current and it is mainly affected by polarization phenomena within the material, whereas the imaginary part of the permittivity takes into account the polarization losses inside the material. Fig. 10d reports the real part of the complex permittivity as function of the fillers content up to a total of 6 wt%, i.e. for the sample whose values of resistivity fall in the measurable range of the instrument. Results show that dielectric permittivity (i.e. ε') increases respect to that of pure PLA with the addition of filler, which has been attributed to the polarization of the matrix/filler interface and/or the polarization of the conductive particles [56]. This increase becomes particularly significant when the concentration of filler exceeds the electrical percolation threshold as in the case of 1.5 wt% MWCNT/PLA and 1.5 wt% MWCNT/1.5 wt% GNP/PLA that exhibit, respectively, a permittivity (at 100Hz) of 46 and 125 whereas only 4.8 is measured for unfilled PLA. Due to their high breakdown strength and other remarkable mechanical, thermal and chemical properties, neat polymers are promising dielectric materials for charge storage applications. However, low value of relative permittivity (i.e. ε') hinders their practical applications. Therefore, in the light of the results, polymer nanocomposites may be a solution in overcoming such limitation since the introduction of small amount of nanofillers can increase ε' of resulting materials without sacrificing the remaining properties typical of the host matrix.

4. Conclusions

A comprehensive study was performed on the rheology, morphology and electrical properties of the poly-lactic acid (PLA) filled with carbon-based particles such as multi-walled carbon nanotubes (MWCNTs), graphene nanoplates (GNPs) and a combination of both fillers. Comparable values for the percolation threshold are found by means of rheological and electrical studies. The experimental results reveal value of the electrical conductivity of the order of

some S/m for filler amounts of 12 wt% that does not compromise the viscosity of the polymer. A good stability of the electrical properties are found in the investigated frequency range (i.e 100Hz÷1MHz). Current 3D printing limitations can be overcome with the development of the novel formulation of nanocarbon/poly(lactic) acid with different percentages of carbon nanostructures. Such systems allow improved electromagnetic properties, customizable properties, specific multifunctionality and lower cost over traditional materials.

Thermal characteristics and the electromagnetic response properties—absorption, reflection, and transmission coefficients—at microwave and THz frequencies of these type of composites have been also investigated by the authors in previous studies [57, 58]. It is found that the incorporation in the PLA matrix of carbonaceous nanostructures with predominantly two-dimensional shape such as GNPs, significantly improves the thermal conductivity and then the heat conduction in the resulting composites [57], whereas the best EM absorption (69%) and EM efficiency (96%) were shown by multiphase system (6 wt% of total charge) [58]. Therefore, high electrical conductivity values, remarkable thermal conductivity and good EM properties are favourable elements for making these materials suitable for packaging use with EM shielding properties where ability to dissipate in heat the incident wave is required.

Nowadays the microwave spectrum becomes more and more crowded due to the increasingly massive presence of electronic devices that, if on the one hand they improve our everyday life on the other they act as electromagnetic radiation emitters thus perturbing the function of the surrounding devices resulting in an electromagnetic coupling, also known as electromagnetic interference (EMI).

Therefore, various attempts have been taken to address EMI issues, by developing new advanced materials able to absorb or to reflect electromagnetic radiation in certain frequency range. Such materials, characterized by properties mostly found in metals such as by both high electric conductivity and high dielectric constant, can be used as EM coatings, shields, filters and radar absorbing materials (RAMs) [59] that require particular attention in the design process especially in the aerospace industry [60]. In order to increase knowledge in this sector, the experimental characterization discussed in the present study was carried out.

However, the full potential of nanotechnology in the field of 3D printing is not yet fully exploited due to some limitations that must be still resolved. Among them, let's remember the restricted range of materials that can be replicate, difficulties of 3D printing finely-detailed objects and finished product quality issues as well as not enough

mechanical strength as conventionally manufactured parts. Moreover, the economic aspect, especially when using these nanomaterials in order to print electrically conductive parts, is not negligible.

Future work will attempt to find, by means of Robust Design (RD) approach, the best combination of the two fillers in order to improve the overall performances of the resulting materials with the lower content of fillers thus improving their cost-effectiveness [61]. Furthermore, potential correlations between mechanical and electrical properties will be investigated both experimentally and numerically in an ongoing work similarly to previous studies of the authors based on different resins loaded with carbon-based nanoparticles [62, 63].

Acknowledgments

This work was carried out within the framework of the Marie Skłodowska-Curie Actions (MSCA) Research and Innovation Staff Exchange (RISE) H2020-MSCA-RISE-2016, Project Acronym: Graphene 3D – Project Number: 734164. The support from H2020-SGA-FET-GRAPHENE 2017-785219 Graphene FET Flagship Core2 is also acknowledged.

References

[1] W. Zhang, A. A. Dehghani-Sanij, and R. S. Blackburn. Carbon based conductive polymer composites. J. Mater. Sci. 42 (2007) 3408-3418.

[2] J. Cha, G. H. Jun, J. K. Park, J. C. Kim, H. J. Ryu, S. H. Hong. Improvement of modulus, strength and fracture toughness of CNT/Epoxy nanocomposites through the functionalization of carbon nanotubes. Compos. Part B 129 (2017) 169-179.

[3] L. Vertuccio, L. Guadagno, G. Spinelli, S. Russo, G. Iannuzzo Effect of carbon nanotube and functionalized liquid rubber on mechanical and electrical properties of epoxy adhesives for aircraft structures: Compos. Part B 129 (2017) 1-10.

[4] L. Guadagno, M. Raimondo, V. Vittoria, L. Vertuccio, C. Naddeo, S.Russo, B. De Vivo, P. Lamberti, G. Spinelli and Vincenzo Tucci," Development of epoxy mixtures for application in aeronautics and aerospace" RSC Adv. 4 (2014) 15474-15488.

[5] C.K. Chua, K.F. Leong, 3D Printing and Additive Manufacturing: Principles and Applications, 5th ed., World Scientific, Singapore, 2016.

[6] B. Utela, D. Storti, R. Anderson, M. Ganter. A review of process development steps for new material systems in three dimensional printing (3DP). J. Manuf. Process. 10 (2008) 96-10.

[7] T. D. Ngo, A. Kashani, G. Imbalzano, K. T. Q. Nguyen, D. Hui, Additive manufacturing (3D printing): A review of materials, methods, applications and challenges, Compos. Part B 143 (2018) 172-196.

[8] XinWang, Man Jiang, Zuowan Zhou, Jihu Gou, David Hui, 3D printing of polymer matrix composites: A review and prospective, Compos. Part B 110 (2017) 442-458.

[9] O. Ivanova, C. Williams, T. Campbell. Additive manufacturing (AM) and nanotechnology: promises and challenges. Rapid Prototyping Journal 19 (2013) 353-364.

[10] A. V. Melnikov, M. Shuba, P. Lambin, Modeling the electrical properties of 3D printed meshes with the theory of resistor lattices, Phys. Rev. E 97 (2018) 043307-11.

[11] J. G. Bai, K. D. Creehan, H.A. Kuhn. Inkjet printable nanosilver suspensions for enhanced sintering quality in rapid manufacturing, Nanotechnology 18 (2007) 185701-185705.

[12] P. Buffat, J. P. Borel. Size effect on the melting of gold particle. Phys. Rev. A, 13 (1976) 2287-2298.

[13] J. J. Beaman, C. R. Deckard, Patent 4938816 A, 1990.

[14] S. Z. Guo, F. Gosselin, N. Guerin,A. M. Lanouette, M. C. Heuzey, D. Therriault..Solvent-Cast Three-Dimensional Printing of Multifunctional Microsystems. Small 9 (2013) 4118-4122.

[15] L. L. Lebel, B. Aissa, M. A. E. Khakani, D. Therriault. Ultraviolet-Assisted Direct-Write Fabrication of Carbon Nanotube/Polymer Nanocomposite Microcoils. Adv. Mater. 22 (2010) 592-596.

[16] X. Zhang, X. N. Jiang, C. Sun. Micro-stereolithography of polymeric and ceramic microstructure. Sens. Actuators A. 77 (1999) 149-146.

[17] S. J. Leigh, R. J. Bradley, C. P. Purssell, D. R. Billson, D. A. Hutchins. A simple, low-cost conductive composite material for 3D printing of electronic sensors. PloS one, 2012; 7, e49365.

[18] X. Wei, D. Li, W. Jiang, Z. Gu, X. Wang, Z. Zhang, Z. Sun. WEI, Xiaojun, et al. 3D printable graphene composite. Sci. Rep. 5 (2015) 11181.

[19] S.S. Crump. Apparatus and method for creating three-dimensional objects. U.S. Patent No 5,121,329, 1992.

[20] C. Zhao, C. Wang, R. Gorkin III, S. Beirne, K. Shu, G. G. Wallace. Three dimensional (3D) printed electrodes for interdigitated supercapacitors Electrochem. Commun. 41 (2014) 20-23.

[21] A. Ambrosi, J. G. S. Moo, M. Pumera. Helical 3D-Printed Metal Electrodes as Custom-Shaped 3D Platform for Electrochemical Devices. Adv. Funct. Mater. 26 (2016) 698-703.

[22] J. J. Adams, E. B. Duoss, T. F. Malkowski, M. J. Motala, B. Y. Ahn, R. G. Nuzzo, J. T. Bernhard, J. A. Lewis. Conformal printing of electrically small antennas on three-dimensional surfaces. Adv. Mater. 23 (2011) 1335-1340.

[23] S. Z Guo, X. Yang, M. C. Heuzey, D. Therriault. 3D printing of a multifunctional nanocomposite helical liquid sensor. Nanoscale, 7 (2017) 6451-6456.

[24] K. Sun, T.-S. Wei, B.Y. Ahn, J.Y. Seo, S.J. Dillon, J.A. Lewis. 3D printing of interdigitated Li-Ion microbattery architectures Advanced Materials 25 (2013) 4539-4543.

[25] R. H. Sanatgar, C. Campagne, V. Nierstrasz, Investigation of the adhesion properties of direct 3D printing of polymers and nanocomposites on textiles: Effect of FDM printing process parameters. Appl. Surf. Sci. 403 (2017) 551-56.

[26] J. Bustillos, D. Montero, P. Nautiyal, A. Loganathan, B. Boesl, A. Agarwal, Integration of Graphene in Poly(Lactic) Acid by 3D Printing to Develop Creep and Wear-Resistant Hierarchical Nanocomposites, Polymer Compos. (2017) 1-12, DOI: 10.1002/pc.24422.

[27] T. T. L. Ferreira, I: C. Amatte, T. A. Dutra, D. Bürger, Experimental characterization and micrography of 3D printed PLA and PLA reinforced with short carbon fibers, Compos. Part B, 124 (2017) 88-100].

[28] S. W. Kwok, K. H. H. Goh, Z. D. Tan, S. T. M. Tan, W. W. Tjiu, J. Y. Soh, K. E. J. Goh,. Electrically conductive filament for 3D-printed circuits and sensors. Appl. Mater. Today, 9 (2017) 167-175.

[29] G. Alaimo, S. Marconi, L. Costato, F. Auricchio, Influence of meso-structure and chemical composition on FDM 3D-printed parts, Compos. Part B, 113 (2017) 371-380.

[30] U Kalsoom, PN Nesterenko, B Paull. Recent developments in 3D printable composite materials. RSC Adv. 6 (2016) 60355-60371.

[31] B.I Oladapo, A. O. M. Adeoye, M. Ismail, Analytical optimization of a nanoparticle of microstructural fused deposition of resins for additive manufacturing, Compos. Part B (2018), doi: 10.1016/j.compositesb.2018.05.041.

[32] D. Stoof, K. Pickering, Sustainable composite fused deposition modelling filament using recycled pre-consumer polypropylene, Compos. Part B 135 (2018) 110-118.

[33] R. Ivanova, R. Kotsilkova. Rheological study of poly(lactic) acid nanocomposites with carbon nanotubes and graphene additives as a tool for materials characterization for 3D printing application. Appl. Rheol. 28 (2018), 54014, doi: 10.3933/ApplRheol-28-54014.

[34] D. Bychanok, S. Li, G. Gorokhov, 1 K. Piasotski, 1 D. Meisak, P. Kuzhir, E.A. Burgess, C.P. Gallagher, F.Y. Ogrin, A.P. Hibbins, A. Pasc, A. Sanchez-Sanchez, V. Fierro, and A. Celzard Fully carbon metasurface: absorbing coating in microwaves, J. Appl. Phys. 121(16):165103-1 – 165103-9.

[35] H.M. Hassanabadi, M. Wilhelm, D. Rodrigue. A rheological criterion to determine the percolation threshold in polymer nano-composites. Rheol Acta 53 (2014) 869–882.

[36] G. Heinrich, M. Klüppel, TA Vilgis. Reinforcement of elastomers. Curr. Opin. Solid State Mater Sci. 6 (2002) 195–203.

[37] R. Buscall, P.D.A. Mills, J.W. Goodwin, D.W. Lawson. Scaling behavior of the rheology of aggregate network formed by colloidal particles. J. Chem. Soc. Faraday Trans. 84 (1998) 4249-4260

[38] R. Kotsilkova. Thermosetting nanocomposites for engineering application. Smithers Rapra Technology, UK, 2007.

[39] J-M Piau, M. Dorget, J-F. Palierne, A. Pouchelon. Shear elasticity and yield stress of silica–silicone physical gels: fractal approach. J Rheol. 43 (1999) 305–314.

[40] I. Balberg, N. Binenbaum, N. Wagner. Percolation thresholds in the three-dimensional sticks system. Phys. Rev. Lett. 52 (1984) 1465–1468.

[41] De Vivo B, Lamberti P, Spinelli G, Tucci V. Numerical investigation on the influence factors of the electrical properties of carbon nano tubes-filled composites. J. Appl Phys 113 (2013) 244301-12.

[42] C. Penu, G-H Hu, A. Fernandez, P. Marchal, L. Choplin. Rheological and Electrical Percolation Thresholds of Carbon Nanotube/Polymer Nanocomposites. Polym. Eng. Sci. 52 (2012) 2173–2181.

[43] A. Zohrevand, A. Ajji, F. Mighri. Relationship between rheological and electrical percolation in a polymer nanocomposite with semiconductor inclusions. Rheol Acta 53 (2014) 235–254.

[44] A. K. Kota, B. H. Cipriano, M. K. Duesterberg, A. L. Gershon, D. Powell, S. R. Raghavan, H. A. Bruck. Electrical and Rheological Percolation in Polystyrene/MWCNT Nanocomposites. Macromolecules 40 (2007) 7400-7406.

[45] B. De Vivo, P. Lamberti, G. Spinelli, V. Tucci, A morphological and structural approach to evaluate the electromagnetic performances of composites based on random networks of carbon nanotubes, J. Appl. Phys. 115 (2014) 154311.

[46] K. Gnanasekaran, T Heijmans, S. van Bennekom, H. Woldhuis, S. Wijnia, G. de With, H. Friedrich. 3D printing of CNT- and graphene-based conductive polymer nanocomposites by fused deposition modeling. Appl. Mater. Today 9 (2017) 21–28

[47] J. Urquijo, S. Dadreou, G. Guerrica_Echevarria, J. I.. Eguiazabal. Morphology and properties of electrically and rheologically percolated PLA/PCL/CNT nanocompoistes. J. Appl. Polym. SCi. 134 (2017) 45265-10.

[48] C. –W. Nan, Y. Shen Y and J. Ma. Physical Properties of Composites Near Percolation Annu. Rev. Mater. Res. 40 (2010) 131–51.

[49] L. Guadagno, C. Naddeo, M. Raimondo, G. Barra, L. Vertuccio, S. Russo, K. Lafdi, V. Tucci, G. Spinelli, and P. Lamberti. Influence of carbon nanoparticles/epoxy matrix interaction on mechanical, electrical and transport properties of structural advanced materials. Nanotechnology 28 (2017) 094001 (20pp).

[50] M. T. Connor, S. Roy, T. A. Ezquerra and F. J. B. Calleja. Broadband ac conductivity of conductor-polymer composites Phys. Rev. B 57 (1998) 2286-2294.

[51] A. Mdarhri, F. Carmona , C. Brosseau C and P. Delhaes. Direct current electrical and microwave properties of polymer-multiwalled carbon nanotubes compositesJ. Appl. Phys. 103 (2008) 054303

[52] B. E. Kilbride, J. Coleman, J. Fraysse, P. Fournet, M. Cadek, A. Drury, S. Hutzler, S. Roth S and W. Blau. J. Experimental observation of scaling laws for alternating current and direct current conductivity in polymer-carbon nanotube composite thin films Appl. Phys. 92 (2002) 4024–30.

[53] B. De Vivo, P. Lamberti, G. Spinelli, V. Tucci, L. Guadagno and M. Raimondo. The effect of filler aspect ratio on the electromagnetic properties of carbon-nanofibers reinforced composites, J. Appl. Phys. 118 (2015) 064302.

[54] J.C. Dyre, The random free-energy barrier model for ac conduction in disordered solids, J. Appl. Phys. 64 (1988) 2456-2468.

[55] D. Almond, G. Duncan, A. West, The determination of hopping rates and carrier concentrations in ionic conductors by a new analysis of ac conductivity, Solid State Ionics 8 (1983) 159-164.

[56] V. Panwar, J. O. Park, S. H. Park, S. Kumar,R. M. Mehra, Electrical, dielectric, and electromagnetic shielding properties of polypropylene-graphite composites. J. Appl. Polym. Sci. 115 (2010) 1306-1314.

[57] P. Lamberti, G. Spinelli, P. P. Kuzhir, L. Guadagno, C. Naddeo, V. Romano, R. Kotsilkova, P. Angelova, V. Georgiev. Evaluation of Thermal and Electrical Conductivity of Carbon-based PLA Nanocomposites for 3D Printing. In: AIP Conference Proceedings, 2018, pp. 020158-1–020158-4.

[58] G. Spinelli, P. Lamberti, V. Tucci, R. Kotsilkova, S. Tabakova, R. Ivanova, P. Angelova, V. Angelov, E. Ivanov, R. Di Maio, C. Silvestre, D. Meisak, A. Paddubskaya, P. Kuzhir. Morphological, Rheological and Electromagnetic Properties of Nanocarbon/Poly (lactic) Acid for 3D Printing: Solution Blending vs. Melt Mixing. Materials, 11 (2018), 2256/1- 2256/17.

[59] Z. Viskadourakis, K. C. Vasilopoulos, E. N. Economou, C. M. Soukoulis, G. Kenanakis. Electromagnetic shielding effectiveness of 3D printed polymer composites. Appl. Phys. A 123 (2017) 736/1-736/7.

[60] S. Loya1, Habibullakhan. Analysis of Shielding Effectiveness in the Electric Field and Magnetic Field and Plane Wave for Infinite Sheet. International Journal of Electromagnetics and Applications 6 (2016) 31-41.

[61] B. De Vivo, P. Lamberti, G. Spinelli, V. Tucci, L. Guadagno, M. Raimondo, L. Vertuccio, V. Vittoria. Improvement of the electrical conductivity in multiphase epoxy-based MWCNT nanocomposites by means of an optimized clay content". Compos. Sci. Techn. 89 (2013) 69–76.

[62] B. De Vivo, P. Lamberti, G. Spinelli, V. Tucci, L. Vertuccio, and V. Vittoria. Simulation and experimental characterization of polymer/carbon nanotubes composites for strain sensor applications. J. Appl. Phys. 116 (2014) 054307.

[63] L. Vertuccio, L. Guadagno, G. Spinelli, P. Lamberti, V. Tucci and S. Russo. Piezoresistive properties of resin reinforced with carbon nanotubes for health-monitoring of aircraft primary structures. Compos. Part B 107 (2016) 199-202.

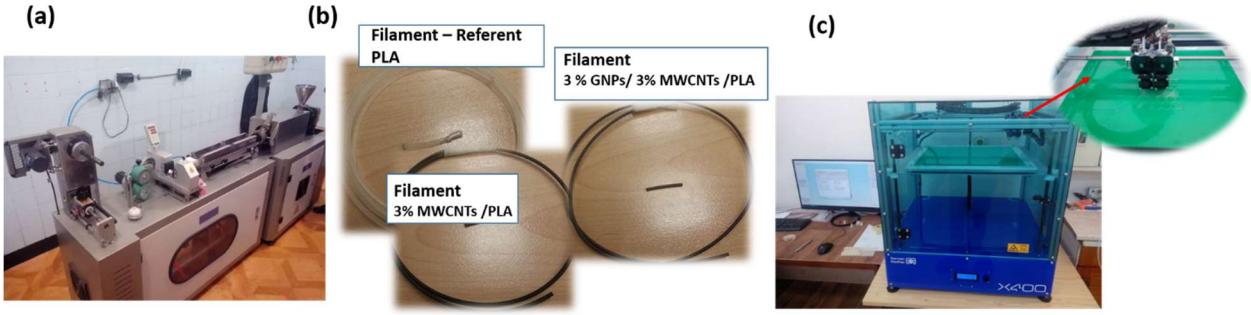

FIGURE 1: a) Plastic filament extruder (Friend Machinery Co.) for the production of suitable filaments (Fig. 1b) to be used with X400 PRO German RepRap 3D printer (Fig. 1c).

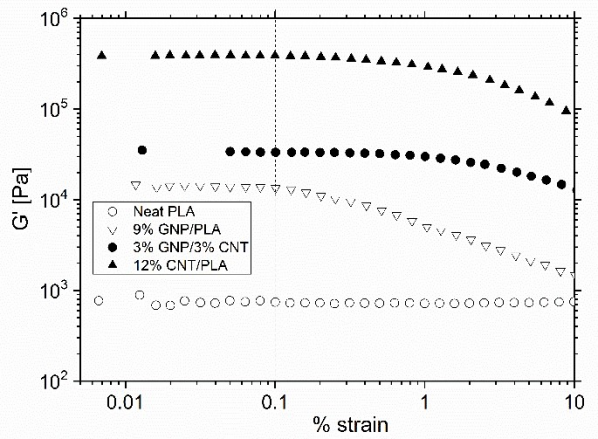

FIGURE 2: Storage modulus, G', versus % strain for the neat PLA and example nanocomposites with 6, 9 and 12 wt% filler content.

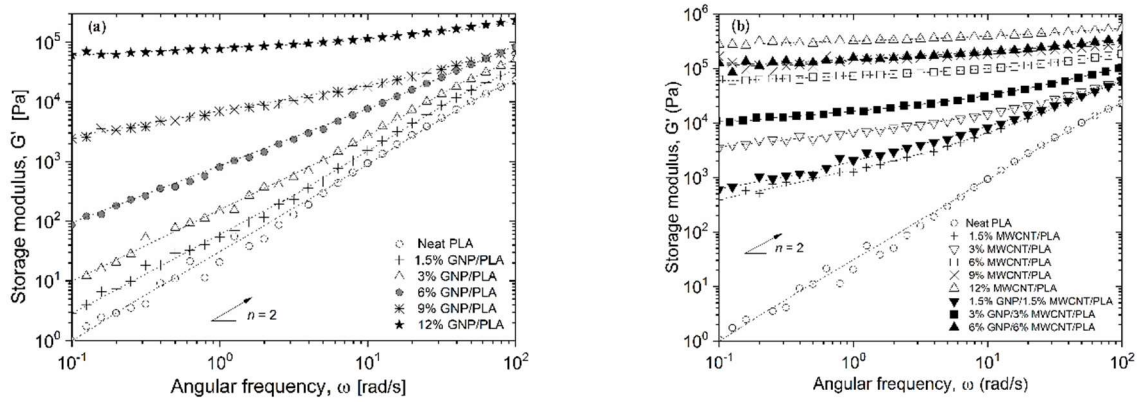

FIGURE 3: Storage modulus, G', versus angular frequency, ω for (a) GNP/PLA and (b) MWCNT/PLA and GNP/MWCNT/PLA composites, with varying the filler contents from 0 to 12 wt%.

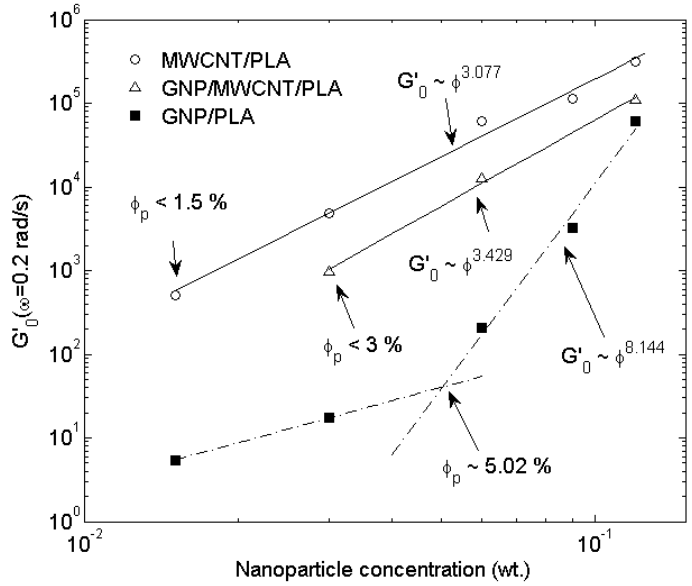

FIGURE 4. Terminal storage modulus $G_o^{'}$ vs. GNP and MWCNTs nanoparticle concentration (wt. parts) for the binary and ternary nanocomposites with PLA matrix polymer. The arrows show the percolation threshold (ϕ_p) and the scaling law of $G_o^{'}$ with parameter (m) for each nanocomposite type.

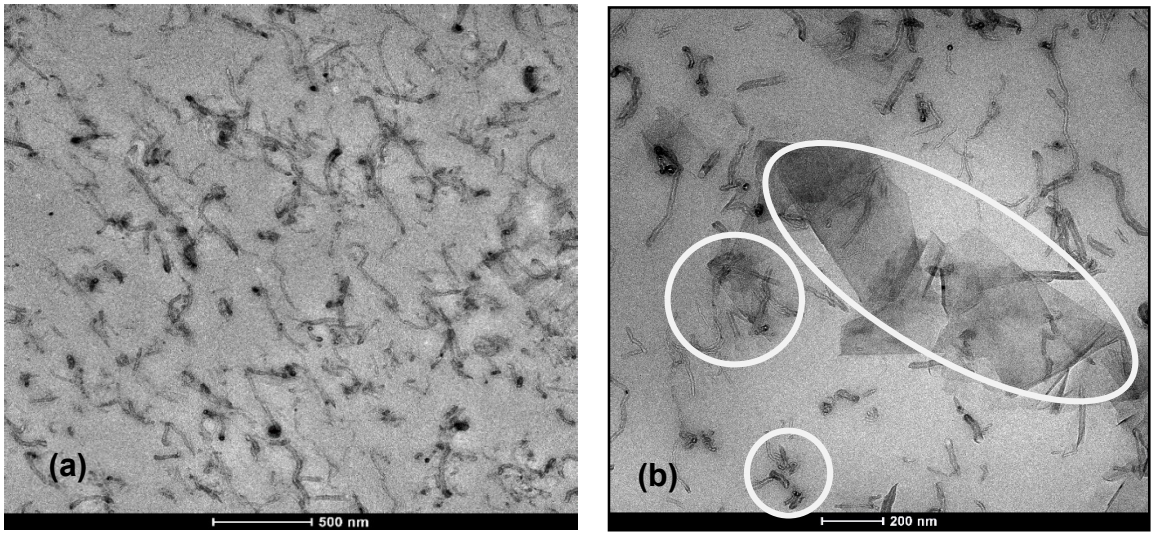

FIGURE 5. TEM micrographs of bi-filler nanocomposite containing 3 wt.% GNP and 3 wt.% MWCNT at (a) low magnification (500 nm scale) and (b) high magnification (200 nm scale). The circles drawn in (b) point the small fractals formed by MWCNT and the mixed fillers MWCNT/GNPs; the ellipse points the large fractal formed by the GNPs.

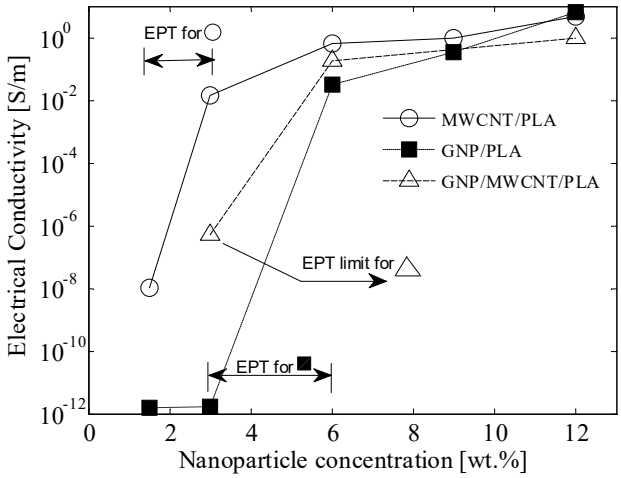

FIGURE 6. Conductivity of nanocomposite systems as a function of the fillers concentrations (wt%).

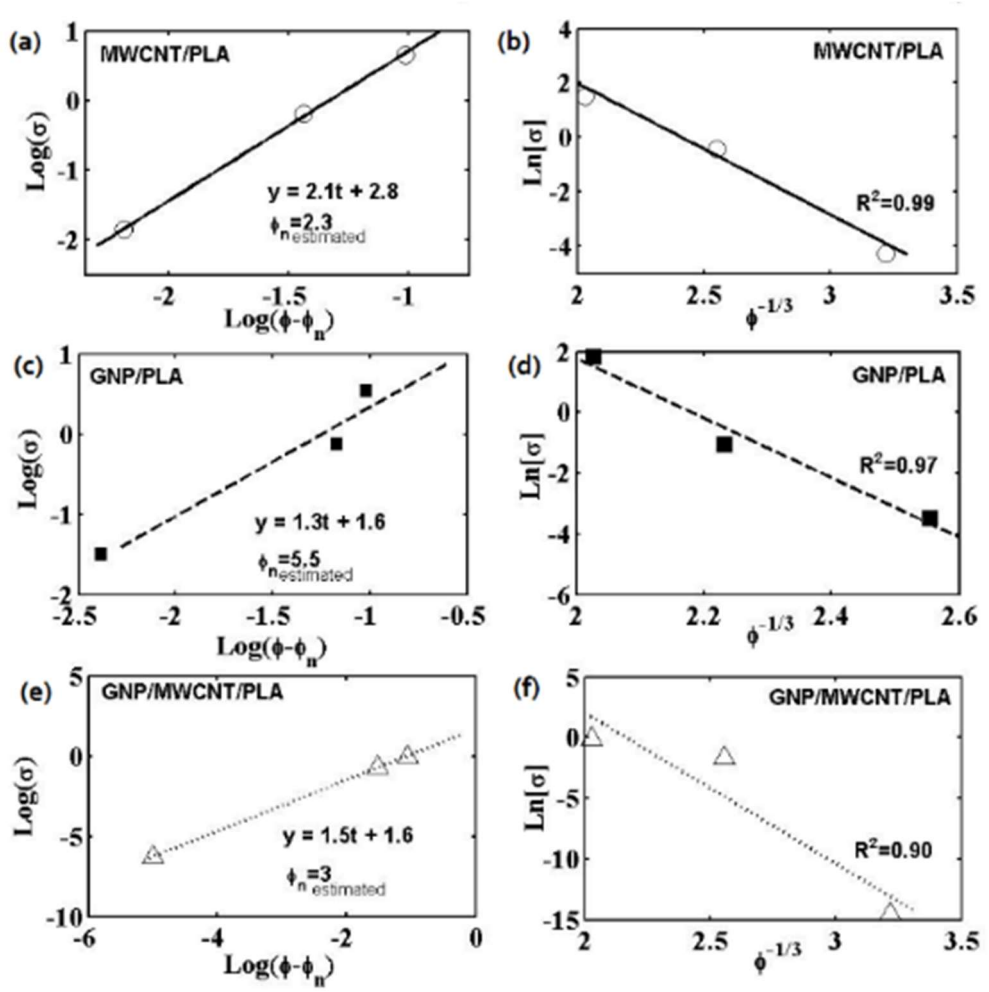

FIGURE 7. Log–log plot of the electrical conductivity as a function of (ϕ-ϕ_n) with a linear fit for composites reinforced with (a) MWCNTs; (c) GNPs; (c) GNPs/MWCNTs (e), respectively. Plot of the natural logarithm of DC conductivity for sample above the EPT vs. $\phi^{-1/3}$ for composites reinforced with (b) MWCNTs; (d) GNPs; (f) GNPs/MWCNTs, respectively. The straight lines fit the DC data (marker) according to equation (5).

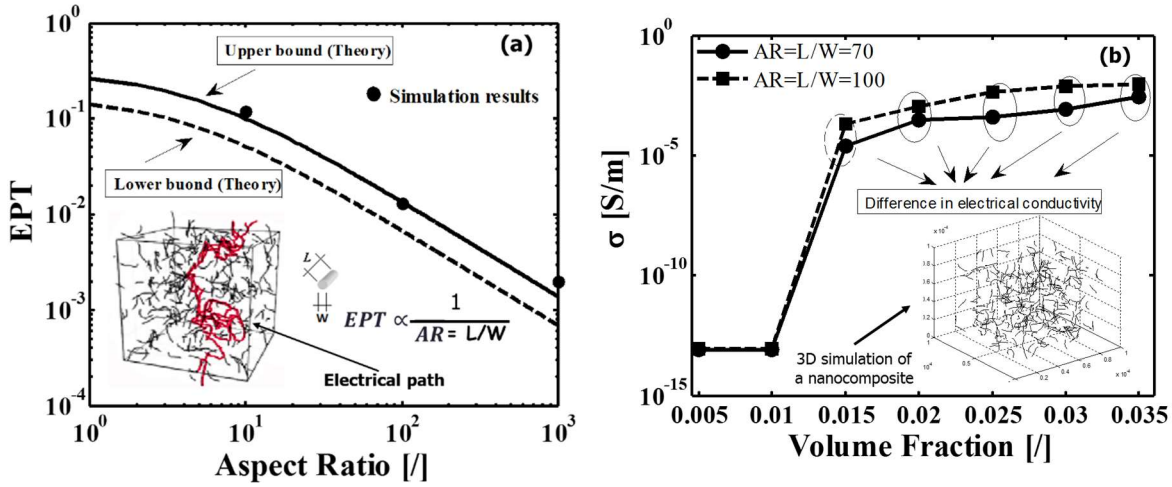

FIGURE 8. Numerical investigation of the influence of the aspect ratio of the inclusions on the electrical percolation threshold (a) and on the electrical conductivity of the nanocomposites (b).

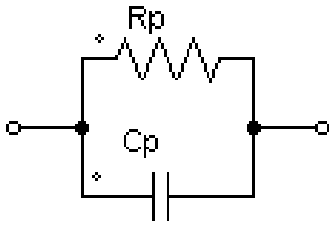

FIGURE 9: Elementary electric circuit of a nanocomposite.

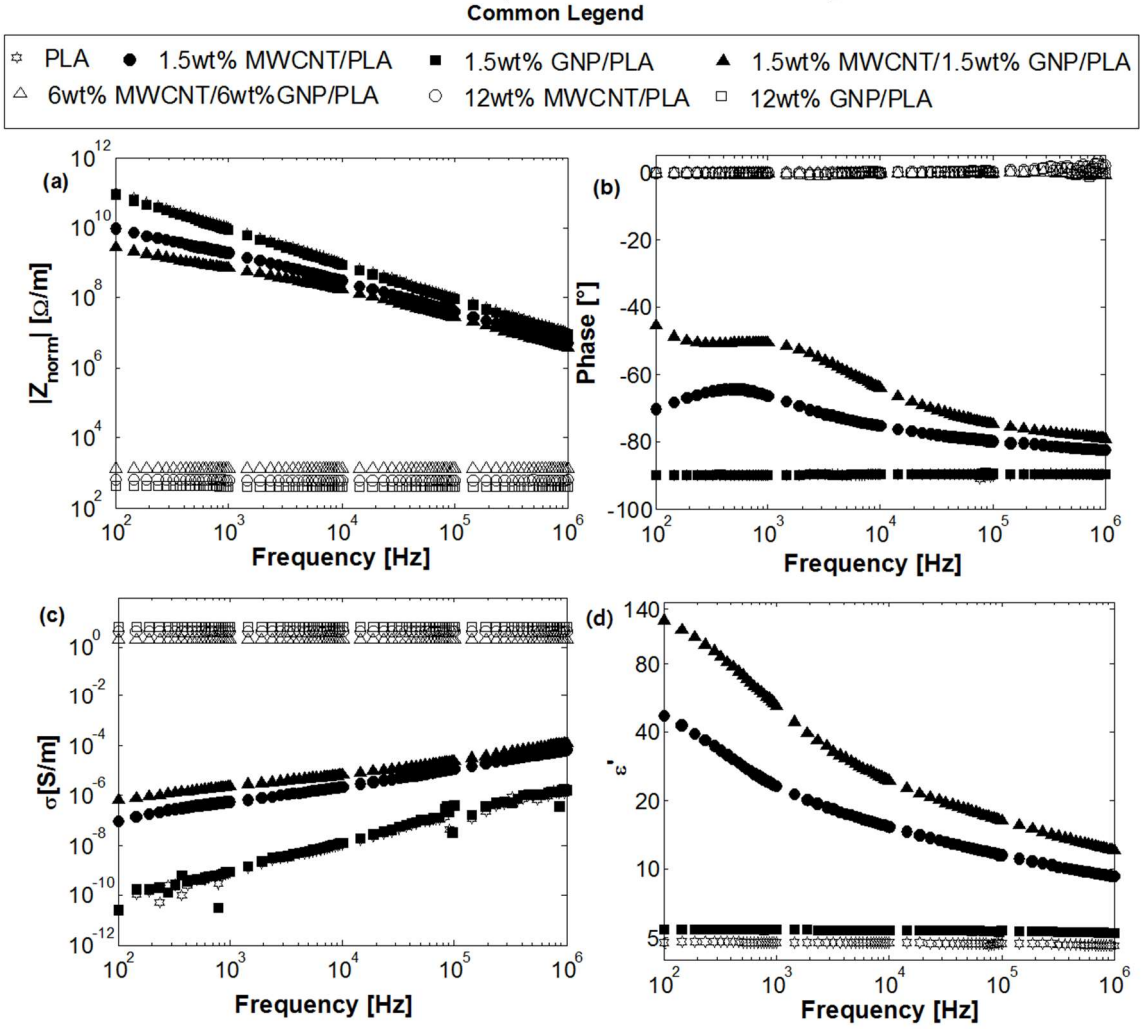

FIGURE 10. AC electrical properties of the samples in the frequency range [100Hz ÷1MHz]: a) normalized impedance with respect to the sample thickness; b) phase impedance (in degree); c) AC electrical conductivity; d) real part of dielectric permittivity.

Table 1. Power law slope (n) of storage modulus

Filler content wt%	Terminal slope (n) of G' (ω), at 0.1-1 s^{-1}		
	GNP/ PLA	MWCNT/ PLA	GNP/MWCNT/PLA (50:50)
0 - Referent PLA	2.0	2.0	2.0
1.5	1. 724	0.527	-
3	1.428	0.262	0.347
6	0.924	0.096	0.200
9	0.437	0.095	-
12	0.126	0.065	0.090
ϕ_p	ϕ_p = 5.02 %	ϕ_p < 1.5 %	ϕ_p < 3 %

Table 2. Terminal storage modulus $G_o^{'}$ vs. GNP and MWCNTs nanoparticle concentration for the binary and ternary nanocomposites with PLA matrix polymer.

Filler content wt%	Terminal storage modulus $G_o^{'}$ (ω=0.2 rad/s)		
	GNP/ PLA	MWCNT/ PLA	GNP/MWCNT/PLA (50:50)
1.5	5.442	569.7	-
3	17.29	5.2305×10^{3}	1021
6	204.50	2.0161×10^{4}	1.1×10^{4}
9	4714	1.121×10^{5}	-
12	6.075×10^{4}	3.4799×10^{5}	1.184×10^{5}

Table 3. DC electrical conductivity at room temperature (average values)

Filler content wt%	σ (S/m)		
	GNP/ PLA	MWCNT/ PLA	GNP/MWCNT/PLA (50:50)
1.5	1.51×10^{-12}	1.08×10^{-8}	-
3	1.71×10^{-12}	1.40×10^{-2}	5.026×10^{-7}
6	3.12×10^{-2}	6.57×10^{-1}	1.856×10^{-1}
9	3.47×10^{-1}	9.40×10^{-1}	-
12	6.27	4.54	9.50×10^{-1}
ϕ_n	[3÷6] wt%	[1.5÷3] wt%	[3÷6] wt%